FISEVIER

Contents lists available at ScienceDirect

Surfaces and Interfaces

journal homepage: www.sciencedirect.com/journal/surfaces-and-interfaces



Spatially correlated stress-photoluminescence evolution in GaN/AlN multi-quantum wells

Fernando M. de Oliveira ^{a,*}, Andrian V. Kuchuk ^a, Pijush K. Ghosh ^a, Morgan E. Ware ^{a,b}, Yuriy I. Mazur ^a, Gregory J. Salamo ^a

ARTICLE INFO

Keywords:
Gallium nitride
Aluminum nitride
Superlattice
Strain
Raman spectroscopy
Photoluminescence

ABSTRACT

In the manufacture of semiconductor devices, cracking of heterostructures has been recognized as a major obstacle for their post-growth processing. In this work, we explore cracked GaN/AlN multi-quantum wells (MQWs) to study the influence of pressure on the recombination energy of the photoluminescence (PL) from the polar GaN QWs. We grow GaN/AlN MQWs on a GaN(0001)/sapphire template, which provides 2.4% tensile strain for epitaxial AlN. This strain relaxes through the generation and propagation of cracks, resulting in a final inhomogeneous distribution of stress throughout the film. The crack-induced strain variation investigated by micro-Raman spectroscopy and X-ray diffraction mapping revealed a correlation between the spacing of the cracks and the amount of strain between them. We have developed a 2D model that allows us to calculate the spatial variation of the in-plane strain in the GaN and AlN layers. The measured values of compressive in-plane strain in the GaN QWs vary from -0.4 % away from cracks, to -0.7 % near cracks. PL from the GaN QWs exhibits a clear correlation to the varying strain resulting in an energy shift of ~ 140 meV. As a result, we can experimentally calculate a pressure coefficient of PL energy of \sim -60.4 meV/GPa for the \sim 7 nm thick polar GaN QWs. This agrees well with the previously predicted theoretical results by Kaminska et al. in 2016 [DOI: 10.1063/ 1.4962282], which were demonstrated to break down for such wide QWs. We will discuss this difference with respect to the reduction in both the expected point defects and extended defects resulting from not doping and growth on a GaN template, respectively. As a result, our work indicates that cracks can be utilized for investigating some fundamental material properties related to strain effects.

1. Introduction

Semiconductor nanostructures are driving the frontiers of breakthrough technologies across a wide range of industries [1]. In particular, III-nitride materials such as aluminum gallium nitride (AlGaN) alloys and GaN/AlN heterosystems offer exciting prospects for a diverse array of research and device applications including: deep ultraviolet photodetectors [2], piezoelectronics [3], quantum emitters [4], resonant tunneling diodes [5], high-electron-mobility transistors [6] and light emitting diodes [7]. Despite advances in nanoengineering, the fabrication of these nanomaterials is challenging due to the 2.4% in-plane lattice mismatch and the associated stress between GaN ($a_0^{GaN}=3.189\text{Å}$) and AlN ($a_0^{AIN}=3.113$ Å). [8] This is aggravated by the 11% difference between the in-plane thermal expansion coefficients ($\alpha^{GaN}=3.113$).

 $5.11\times 10^{-6}\,K^{-1}$ or $^{AlN}=5.72\times 10^{-6}\,K^{-1}$) [9]. By monitoring the stress in these structures during growth, studies have shown that this interfacial lattice mismatch can lead to misfit dislocations and the formation of cracks in III-V heterostructures as a mechanism of stress relief, altering the material properties [10–13]. However, the use of an AlN buffer has been demonstrated to suppress micro-crack generation in ultra-thin GaN/AlN multi-quantum wells (MQWs), [14] and it has been shown that the propagation of cracks can be prevented by performing nanostructure growth under Ga rich conditions [15].

Superlattices (SLs) are excellent structures to study the effects of strain build-up and relaxation, because in addition to the inherent SL-to-substrate lattice misfit significantly affecting the mechanisms of strain relaxion of these structures, the very thin layers make them extraordinarily sensitive to conditions of strain [16]. Even in the absence of strain, the natural lack of inversion symmetry and the contraction along

E-mail address: fmaiade@uark.edu (F.M. de Oliveira).

^a Institute for Nanoscience and Engineering, University of Arkansas, Fayetteville, AR 72701, USA

^b Department of Electrical Engineering, University of Arkansas, Fayetteville, AR 72701, USA

^{*} Corresponding author.

the c-axis in III-nitrides lead to expressive effects of spontaneous polarization, which create a periodic separation of charges along the growth direction in a SL heterostructure similar in strength and structure to common ferroelectric perovskites [17].

In the presence of stress, the additional strain-induced piezoelectric fields mask the forward-backward band asymmetry of GaN/AlN heterojunctions [18], promoting a polarization dependent band offset that alters the luminescent energy of these structures [19]. The resulting energy shift of the excitonic emission due to the piezoelectric field, known as quantum-confined Stark effect (QCSE), is therefore of great consequence in III-nitride heterostructures [20]. In particular, the band structure engineering of III-nitride SLs via the QCSE has allowed the optimization of blue-green light emitting diodes with improved quantum efficiency by enhancing wavefunction overlap [21]. Usually, investigation of the QCSE through the study of pressure-induced changes to the luminescence is performed by submitting the material to hydrostatic pressure in a diamond anvil cell [22]. The application of hydrostatic pressure is a valuable method in the investigation of band-to-band transitions in single crystals [23,24]. However, in the case of MQWs, the strain in these structures is not hydrostatic, since the stress along axial and in-plane directions differ from each other. The built-in electric field resulting from the crystal polarization along the c-axis changes the shape of the band structure in the QW, resulting in a shift in transition energies. Furthermore, this allows for the tuning of the emission energy in MQWs structures to achieve a desired optical response to pressure, according to the size of the confined region. The dependence on the well thickness for this response has been described in theoretical calculations for GaN/AlN SLs, spanning across a range from almost 30 meV/GPa to -70 meV/GPa by increasing the confinement width of the QW from 1 nm to 6 nm. However, experimental results that follow the predicted trend for confinement widths larger than 5 nm are yet to be obtained [22].

Cracked SLs, alternatively, offer the opportunity of probing the optical properties of a structure which is already displaying a naturally diverse profile of stress levels, therefore not requiring the application of external pressure, regardless of the QW confinement width. [25] In wurtzite crystals, the in-plane cracking pattern runs along crystallographic directions of six-fold symmetry, creating a mosaic of crack lines angularly separated by multiples of $\pi/3$ [25]. The investigation of cracked nitride semiconductors grown on group-IV substrates, such as Si, has indicated a significant effect of the in-plane tensile stress in the vibrational properties of these materials [8,26-28]. The study of the fracture-induced strain profile in cracked GaN/AlN heterostructures grown on a group III-V template and its effect on the optical properties at nanoscale, however, is yet to be explored. The rapidly increasing technologies based on nitrides such as 5 G transceiver devices and the energy-saving white LEDs, which offer better performance in comparison with the traditional Si-based devices, has shown the promising future of the III-V materials industry.

The investigation of the mechanical properties of these materials, at micro- and nanoscale, is therefore paramount for advances in the science of high-efficiency devices. Micro-Raman spectroscopy is a valuable technique for reliable and non-destructive analysis of a wide range of micro- and nanomaterials [28]. Due to its ability to assess spatially resolved strain inhomogeneities at a length scale of 1 μm , this technique has been successfully employed in various studies, including histopathological diagnosis [29], geochemistry studies across the globe [30], and most recently on Mars [31]. In this work, we conducted a comprehensive study of the biaxial strain profile in a cracked GaN/AlN superlattice and its impact on structural and optical properties, such as the pressure coefficient of PL energy for polar GaN/AlN MQWs. In doing so we correlated the PL shift with the nonuniform biaxial strain distribution in cracked GaN/AlN. The crack-induced biaxial strain profile was also investigated locally by micro-Raman spectroscopy using a method based on lattice coherency [25], and on average by X-ray diffraction (XRD), while the effect of strain on the optical emission was

demonstrated by PL. Through the analysis of Raman spectra, we were able to determine the local values of in-plane strain, lattice constant, as well as the stress components along different regions of the superlattice. By performing multiple linear mappings across the cracked regions, our findings revealed a correlation between the amount of strain and the spacing between cracks within these areas. By evaluating XRD reciprocal space maps, we found elongated satellite diffraction patterns indicating lattice coherency affected by in-plane lattice cracking, which displayed a clear stress-photoluminescence response. This investigation provides valuable insights into the dynamics of crystal lattices in the presence of fracture. In addition to exploring fundamental properties of nanomaterials in fractured conditions, such as the pressure coefficient of the bandgap change, we have investigated an extension of the one-dimensional model of strain profile to incorporate a two-dimensional non-parallel arrangement of cracks. The outcome of this research offers a foundation for future studies on III-nitride semiconductors, demonstrating a versatile approach which can be applied to other nanomaterials.

2. Experiment

The growth of a GaN/AlN superlattice (SL) on a GaN-on-sapphire substrate was carried out using plasma-assisted molecular beam epitaxy (PAMBE). The substrate consisted of a ~3 µm thick unintentionally doped layer of GaN(0001) grown on ~100 nm of AlN on Al₂O₃ by hydride vapor phase epitaxy. To enhance substrate heating during growth, a 1 µm layer of titanium was deposited on its backside. Prior to growth, the substrate was cleaned using sonication in acetone, methanol, and isopropanol, and then introduced into the vacuum system through a load-lock and baked at 200°C for an hour under a base pressure of $\sim 5.0 \times 10^{-8}$ Torr to eliminate water vapor. It was then transferred to an outgas chamber with a base pressure of $\sim 5.0 \times 10^{-10}$ Torr, where it was degassed at 300°C for an hour to remove surface contaminants. Finally, the substrate was moved to the main growth chamber with a base pressure of $\sim 1.0 \times 10^{-11}$ Torr for final heat cleaning at 830 °C for an hour. This step prepared the substrate surface for growth and ensured constant heating efficiency. A ~180 nm unintentionally doped GaN buffer layer was grown on the substrate, followed by the growth of a 30-period GaN/AlN superlattice at a temperature of ~795 °C. The thickness of the GaN (7 nm) and AlN (3 nm) layers was kept constant along the entire superlattice. After growth, high-resolution Xray diffraction (HRXRD) measurements were conducted using a Panalytical X'Pert Pro-MRD diffractometer. Micro-Raman measurements were performed at room temperature using a 632.8 nm He-Ne laser and a Horiba Jobin-Yvon LabRam HR800 spectrometer equipped with an electrically-cooled CCD camera and optical microscope. PL experiments were conducted at room temperature using a 266 nm laser as excitation and a nitrogen-cooled CCD camera.

3. Results and discussion

The schematic representation of a slice of the 30-period GaN/AlN superlattice is illustrated in Fig. 1a.

The occurrence of fracture is clearly seen in Fig. 1b, which shows an optical image of an area of $100 \times 100~\mu m^2$ of the surface of the superlattice. The crack propagation closely follows the crystallographic directions [1 $\overline{2}$ 10], [$\overline{11}$ 20] and [1 $\overline{2}$ 10], with statistics with respect to a measured orientational angle shown in Fig. 1c. The observed distribution of the spacing between cracks is also summarized in Fig. 1d, which emphasizes the variety of stress levels the nanosized layers are being submitted to. Likewise, Fig. 1e presents the Gaussian deconvolution of the distribution of values of in-plane lattice constant determined from the HRXRD reciprocal space mapping (RSM) around the asymmetric [$\overline{11}$ 24] reflection shown in Fig. 1f. The presence of a series of satellite reflections in Fig. 1f indicates lattice coherence along the superlattice,

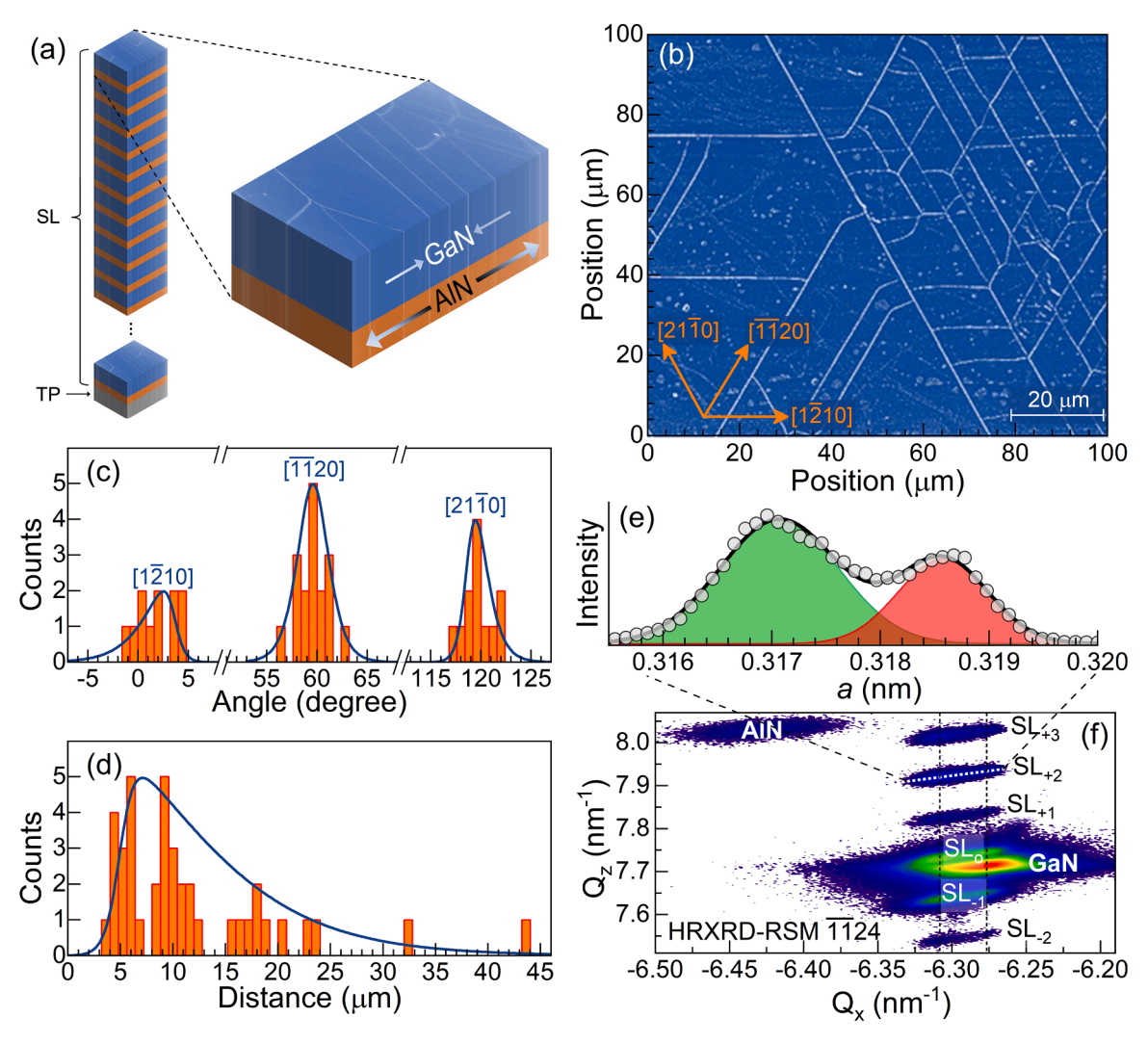


Fig. 1. (a) Scheme of the 30-period GaN/AlN superlattice, where SL indicates the superlattice and TP indicates the template formed by buffer and substrate; (b) Optical image of a $100 \times 100 \,\mu\text{m}^2$ area of the surface of the cracked GaN/AlN superlattice. (c) Distribution of the angular orientation of the cracks of that area relative to the [$1\overline{2}10$] direction, and (d) distance between cracks. (e) Gaussian deconvolution of the distribution of values of in-plane lattice constant determined from (f) HRXRD reciprocal space mapping (RSM) around the asymmetric [$\overline{11}24$] reflection.

while the elongation of each of those satellites as shown in Fig. 1e demonstrates the nearly bimodal variation of the in-plane lattice constant due to the presence of cracks.

Wurtzite III-nitrides, such as GaN, AlN, and InN, belong to the C_{6V} point group. With four atoms per unit cell, these materials display three acoustic $(A_1 + E_1)$ and nine optical $(A_1 + E_1 + 2E_2 + 2B_1)$ zone-center phonon modes, here identified by the Mulliken nomenclature for irreducible representations. In particular, the optical phonons represent outof-phase atomic vibrations leading to oscillating electric dipoles along the crystal with a frequency that is fundamentally dependent on the local features of the lattice, such as strain, carrier concentration and alloy content. The frequency of these modes can be studied by the technique of Raman spectroscopy in order to obtain information about different aspects of these materials. In particular, the doubly degenerated optical mode, E_2 , represents the vibration of nitrogen atoms relative to the metallic cation (E_2^{High}) and vice-versa (E_2^{Low}) . The highfrequency form, E_2^{High} , is the most intense optical mode observed in the traditional backscattering Raman geometry. And, due to the fact that it is very sensitive to the stressed condition of the lattice, measurements of the frequency, ω , of this mode are usually employed in the investigation of strain, determining the in-plane lattice constant, asL, of each constituent material. These quantities are correlated through the linear deformation potential theory, by describing the zone-center vibrational states of the wurtzite crystal in terms of the components of the stress tensor, and therefore to the strain associated to the deformed lattice constant. If the layers are coherently lattice-matched, the same in-plane a_{SL} is maintained along the entire structure [25]. Eq. (1) illustrates this relationship for the case of a strained wurtzite crystal, which when relaxed displays an in-plane lattice constant a_0 with the E_2^{High} Raman mode at the frequency ω_0 .

$$a_{SL} = a_{0, j} \left[1 + \frac{\omega - \omega_0}{2 \left(a - \frac{bC_{13}}{C_{33}} \right)} \right]_{i}$$
 (1)

Here, $j = \{\text{GaN, AlN}\}\$ identifies the material of the layer of the coherently lattice-matched superlattice, a and b are the deformation potentials, and C_{13} and C_{33} are the elastic constants. Table 1 summarizes the values of these parameters for wurtzite GaN and AlN [25–27].

The presence of fractures modifies the strained condition of the crystal and creates gradients of stress relief across the film, that reduces the in-plane tensile (compressive) strain in the AlN (GaN) layers in the vicinity of every crack. As a consequence, the areas surrounded by lines of cracks exhibit a local maximum value of the in-plane lattice constant

Table 1 Values of relaxed lattice constant (a_0), relaxed frequency of E_2^{High} mode (ω_0), deformation potentials (a and b) and elastic constants (C_{11} , C_{12} , C_{13} and C_{33}) of bulk AlN and GaN.

III-nitride	a ₀ (nm)	(cm^{-1})	$a \ (cm^{-1})$	$b \ (cm^{-1})$	C ₁₁ (GPa)	C ₁₂ (GPa)	C ₁₃ (GPa)	C ₃₃ (GPa)
AlN	0.3113	656.7	-1011	-940	396	137	108	373
GaN	0.3189	567.4	-806	-765	367	135	103	405

exactly halfway between cracks, representing regions of minimum stress relief. To investigate this relationship between biaxial strain and fracture, Fig. 2a shows an area of the GaN/AlN superlattice containing parallel cracks, with a central region about 20 μ m wide separated by two lines of crack. The Raman spectrum acquired exactly on a crack is shown in Fig. 2b, displaying the out-of-plane transverse optical Raman mode $A_1(TO)$ of GaN near 560 cm^{-1} , indicated by an asterisk; as well as the in-

plane E_2^{High} Raman modes of GaN template ($\sim 570~cm^{-1}$), GaN superlattice layer ($\sim 580~cm^{-1}$), AlN superlattice layer ($\sim 610~cm^{-1}$) and AlN template ($\sim 660~cm^{-1}$).

As seen in Fig. 2c-g, which shows the observed change in the Raman spectrum at different positions across a region bounded by the two parallel cracks, the E_2^{High} mode of the superlattice layers exhibits exceptional sensitivity to how far the probed point is from the line of

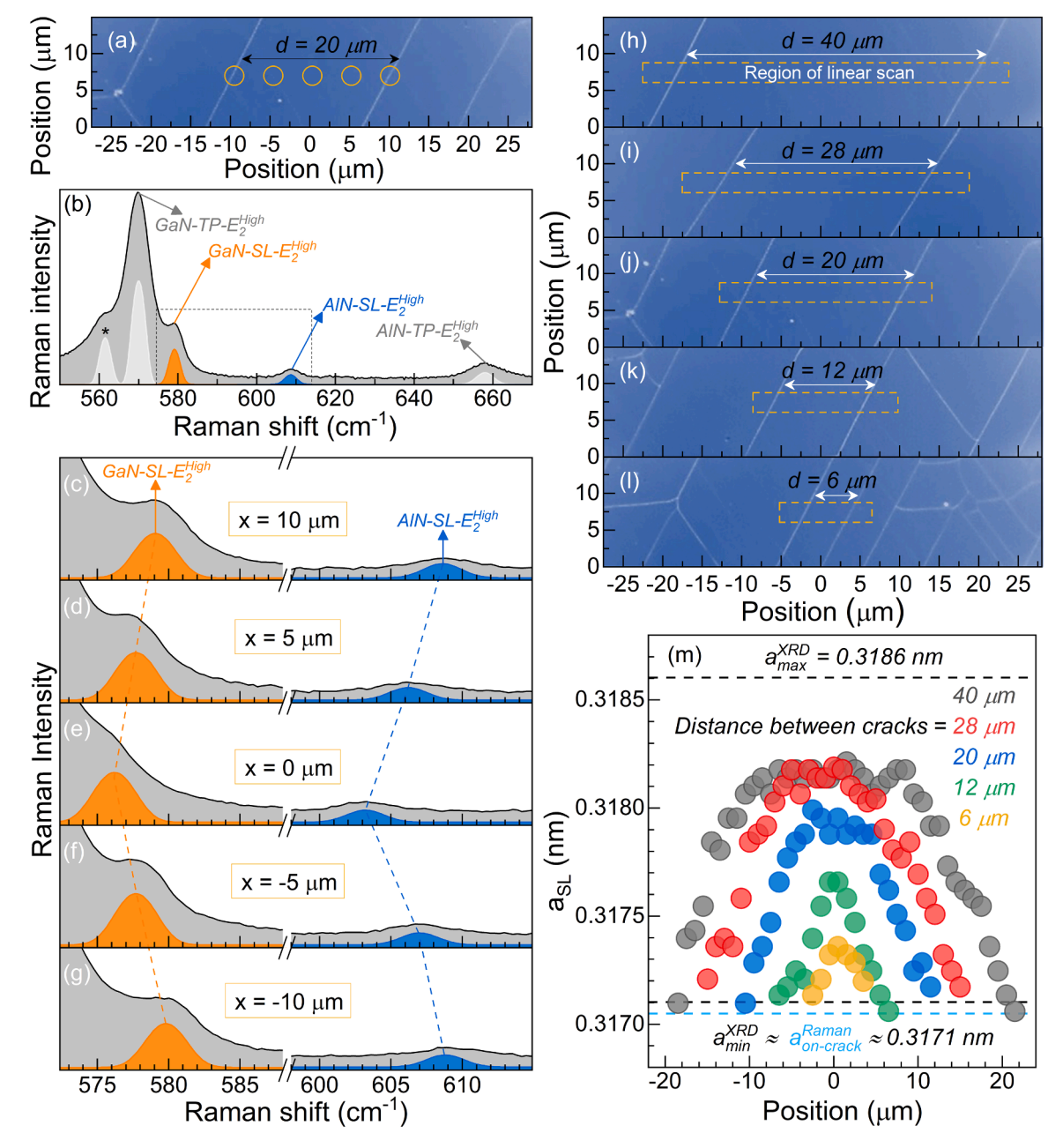


Fig. 2. (a) Optical image of the analyzed area of point scan of the GaN/AlN superlattice, the probed locations are indicated by circles; (b) Raman spectrum acquired on a crack, and (c)-(g) at different positions between cracks. (h)-(l) Optical images of the analyzed areas of linear scan with different distances between cracks, (m) evolution of the in-plane lattice constant a_{SL} of the superlattice.

fracture. In order to investigate the influence of the distance between cracks on the strain profile of the enclosed region, Fig. 2h-l presents five areas displaying different spacing between the lines of fracture, with lengths of approximately 6 μ m to 40 μ m. The evolution of the in-plane lattice constant, a_{SL} , of the superlattice calculated from Eq. (1) is shown in Fig. 2m, ranges from 0.3168 nm to 0.3180 nm. It is evident that the largest values of in-plane lattice constant are seen within the central area away from the lines of cracks. This is caused by the residual tensile strain in the AlN layers that was only minimally released in locations away from the cracks, creating a negative (positive) gradient of tensile (compressive) stress in the AlN (GaN) towards the line of crack. In the presence of parallel lines of fracture, the crack-induced in-plane stress σ at a position x between cracks can be determined using the one-dimensional shear-lag model for axial stiffness by: [32,33]

$$\sigma(x) = \sigma_R + \sigma_S[\tanh(\beta d / 2)\sinh(\beta x) - \cosh(\beta x) + 1]$$
 (2)

Here, σ_R is the residual stress at the crack tip; σ_S is the saturated stress at a location away from cracks; d is the distance between cracks; and β is the shear-lag parameter associated with the efficiency of stress transfer through interfaces [34], which dependents on the shear modulus G = $E/2(1 + \nu)$ of the layer with thickness t, expressed in terms of the Young's modulus $E=\sigma_{\parallel}/\epsilon_{\parallel}=C_{11}+C_{12}-2C_{13}^2/C_{33},$ and on the Poisson's ratio $\nu = C_{13}/(C_{11} + C_{12})$ of the layer [35–37]. For a two-component system formed by film grown on a substrate, the shear-lag parameter β associated to the film is given by β = $\sqrt{(G_F/t_F)\{[2(1-\nu_F^2)/(E_Ft_F)]+[2(1-\nu_S^2)/(E_St_S)]\}}$ Here. [8]. subscript *F* identifies the material of the film layer, while *S* refers to the substrate. However, for a superlattice formed by two layers of different materials periodically alternated and coherently lattice-matched grown on a template formed by buffer and substrate, the cumulative effect of distinct structural parameters at each interface between different materials is quite complex. This can be simplified by evaluating Eq. (2) halfway between lines of cracks, which represents the location of maximum local in-plane lattice constant, $a_{SL}^m = a_{0,j}[1 + (\sigma_i^m/E_j)]$, where j = {GaN, AlN} and m stands for the maximum (minimum) local stress of AlN (GaN). Due to lattice coherency, a_{SL}^m is valid along the entire superlattice. Therefore, the largest in-plane lattice constant represented by the maximum (minimum) in-plane tensile (compressive) stress of the AlN (GaN) superlattice halfway between parallel cracks can be described by:

$$a_{SL}^{m} = a_{SL}^{R} + (a_{SL}^{S} - a_{0,j}) (1 - \operatorname{sech}\{ [(\beta_{j}d)/2] \})$$
 (3)

The derivation of Eq. (3) is detailed in the Supplementary Material file. The evolution of the local largest values of a_{SL} in Fig. 2m, determined by the Raman data using Eq. (1), can be perfectly fitted by Eq. (3) within the range delimited by the in-plane values of lattice constant determined by HRXRD ($a_{min}^{XRD} = 0.3171$ nm, $a_{max}^{XRD} = 0.3186$ nm), resulting in the shearlag parameter $\beta = 0.20 \pm 0.02$ nm⁻¹. This value is very close to the averaged approximation $\beta_{avg} = (1/n) \sum \beta_{A,B} \approx 0.27 \pm 0.05$ nm⁻¹, which accounts for all the n = 60 interfaces olong the entire superalattice, where the value of $\beta_{A,B} = \sqrt{(2G_A/t_A)\{[(1-\nu_A^2)/(E_At_A)] + [(1-\nu_B^2)/(E_Bt_B)]\}}$ of each interface between a layer A with respect to its lower layer B is estimated from the set of mechanical parameters of GaN ($E_{GaN} = 286 \pm 5GPa$, $G_{GaN} = 120 \pm 18GPa$, $v_{GaN} = 0.189 \pm 0.03$) and AlN ($E_{AlN} = 324 \pm 27GPa$, $G_{AlN} = 133 \pm 19GPa$, $v_{AlN} = 0.219 \pm 0.03$) [38], with the individual thicknesses given by $t_{GaN} = 7$ nm and $t_{AlN} = 3$ nm.

As an expansion of the one-dimensional model for the case of multiple lines of non-parallel cracks, we investigated the strain profile of a two-dimensional area of $60\times30~\mu\text{m}^2$ containing a region enclosed by four non-perpendicular lines of crack forming a $36\times23~\mu\text{m}^2$ parallelogram, as indicated in Fig. 3a. In order to obtain the values of the inplane lattice constant within this region, the Raman spectrum was acquired in steps of $\sim1~\mu\text{m}$ along the entire area providing the frequencies of the E_2^{High} mode of AlN and GaN to be used in Eq. (1), resulting in a 2D Raman map of the investigated area. The tensile (compressive) in-plane strain profile, $\epsilon_{xx}^{AlN(GaN)}$, within the AlN (GaN) superlattice layers along the analyzed area is depicted in Fig. 3b-c. It is evident that the maximum values of tensile in-plane strain in AlN are located at the center of the

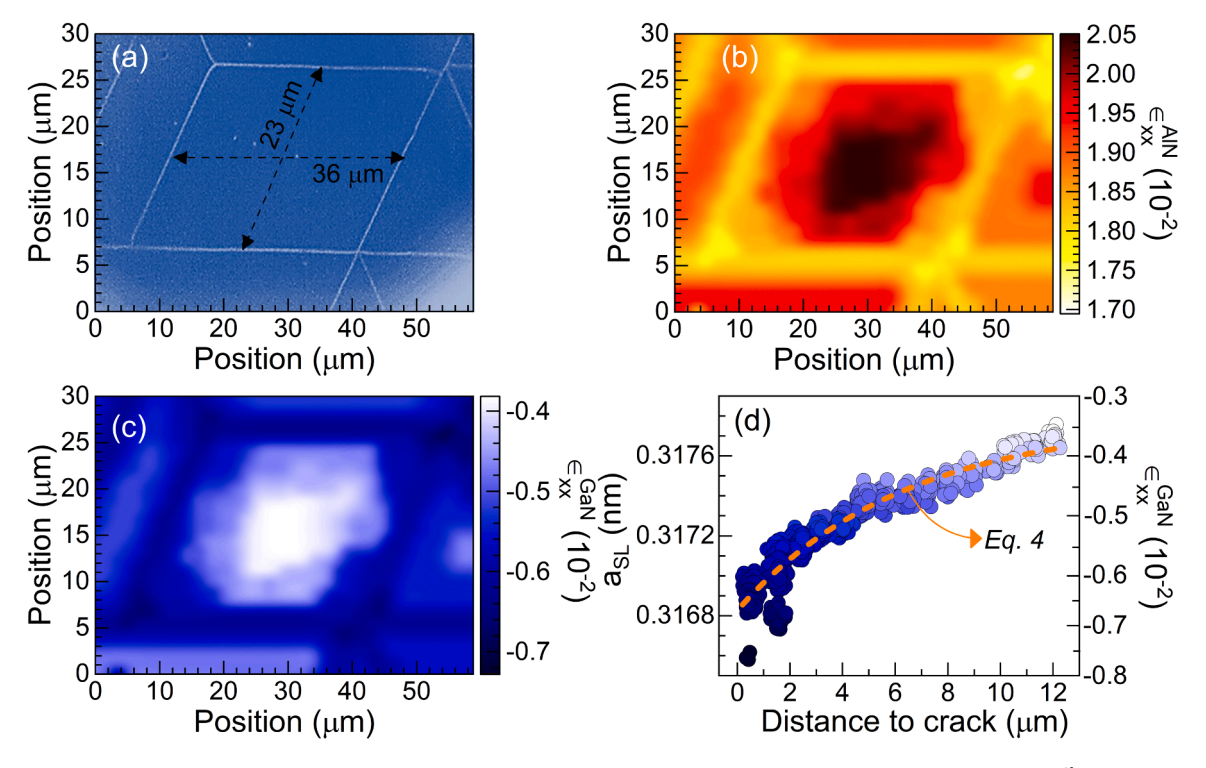


Fig. 3. (a) Optical image of the analyzed areas of two-dimensional scan of the GaN/AlN superlattice; (b) map of in-plane tensile strain $\epsilon_{\chi\chi}^{AlN}$ in the AlN layers and (c) map of in-plane compressive strain $\epsilon_{\chi\chi}^{GaN}$ in the GaN layers along the analyzed area; (d) evolution of the values of in-plane lattice constant a_{SL} and in-plane compressive strain $\epsilon_{\chi\chi}^{GaN}$ in the GaN layers according to the distance to the closest line of crack.

region at locations away from any line of fracture, reaching approximately 2.0 %. A residual in-plane strain of about 1.7 % is also found on the vicinity of the lines of the crack. Similarly, the compressive strain in GaN exhibits values that range from -0.4 % away from cracks, to -0.7 % near cracks.

The in-plane lattice constant at any position of the 2D cracked area can be described by adapting the 1D model defined in Eq. (3), by considering the distance *x* from any location to individual lines of crack:

$$a_{SL}(x) = a_{SL}^{R} + (a_{SL}^{S} - a_{0,j})[\sinh(\beta x) - \cosh(\beta x) + 1]$$
(4)

The derivation of Eq. (4) is detailed in the Supplementary Material file. As seen in Fig. 3d, the values of in-plane compressive strain in the GaN layers of the superlattice calculated from the Raman map data can be very nicely fitted with Eq. (4), which demonstrates the multidimensional applicability of this model. This crack-induced strain diversity modifies the resulting band structure of the GaN/AlN superlattice, creating a non-uniform profile of the electronic potential faced by carriers. As a result, carriers located in areas with low density of lines of crack experience a lower compressive in-plane strain in the GaN layers of the superlattice than the carriers situated in regions of high crack density due to different levels of in-plane tensile stress relief in the AlN layers. This difference in the strained condition modifies the emission energy of the GaN bandgap transitions, as has been shown in crack-free III-nitride heterostructures with different levels of in-plane compressive strain [39]. Theoretical reports have shown that the rate of change in the direct bandgap induced by pressure, $R_n^{\Gamma-HH}$, can be approximated by the negative ratio between the volume deformation potential, $a_{V}^{\Gamma-HH} =$ $dE_{\Gamma-HH}/dln(V)$, of an interband transition between gamma (Γ) and heavy hole (HH) bands, and the bulk modulus, $B = dE_p/dln(V)$, of a direct bandgap semiconductor by $R_p^{\Gamma-HH}=dE_{\Gamma-HH}/dp$ [40,41]. Pressure affects the physical properties of both bulk and nanostructured wurtzite III-nitride materials, influencing at least their lattice constants, bandgap energies and piezoelectrically induced polarization fields [40]. Due to the absence of inversion symmetry in wurtzite crystals, the built-in electric field along the [0001] direction produces an intense spontaneous polarization in hexagonal III-nitride structures. However, in the case of QW structures, this spontaneous polarization is accompanied by an additional strain-induced piezoelectric polarization that modifies the built-in electrical field and leads to a change in the potential felt by carriers, consequently affecting very sensitively the resulting transitions between energy levels, ultimately dominating the effective bandgap of the QW nanostructure. As an example, Strak et al. quantified the pressure-induced variation of the physical properties of GAN/AlN MQWs by analyzing the nonlinear susceptibilities, and obtained distinct pressure dependencies for both bulk and MQW structures [40]. This has been also investigated in detail by Kaminska et al. while studying the essential role of piezoelectric fields on the pressure coefficient of polar MQWs structures [22], and by Teisseyre et al. showing that non-polar GaN QWs exhibited transition energies defined solely by quantum confinement, and similar pressure dependence to bulk GaN [45]. Kaminska et al. showed that non-polar GaN/AlGaN structures of 2-4 nm grown along the a-plane ($\overline{11}20$) direction displayed pressure coefficients of 40-42 meV/GPa, similar to bulk GaN, as opposed to 12-28 meV/GPa for polar GaN/AlGaN structures of same thicknesses grown along c-plane (0001) direction [42]. As the role of the quantum-size Stark effect increases as the thickness of the OWs increases, the predicted values of the pressure coefficient of polar GaN MQWs structures drop rapidly, even becoming negative, as reported by Kaminska et al. from about 24 meV/GPa for 1 nm wide GaN QWs, to almost -60 meV/GPa for 6 nm wide GaN QWs [42]. Experimentally, it is usual to determine the value of the pressure coefficient using one of two methods: by directly applying external pressure on the material using a diamond anvil cell and simultaneously tracking the resulting change in bandgap emission [22]; or else by evaluating the bandgap emission of a set of samples of the same type of material but with different levels of strain [42]. A

cracked superlattice, however, offers the advantage of having in the same sample a continuum gradient of values of strain, which as a result will lead to a gradient of spatially correlated bandgap emissions from the same crystal. This is seen in Fig. 4a that shows the PL emission of the 7 nm GaN layers of the superlattice, which data were acquired at regions of different levels of crack density.

In contrast to the micro-Raman measurements, the probing laser of the PL system used in this study has a spot size that is larger than the spacing of the lowest density cracks. Since the superlattice had a nonuniform distribution of crack densities along the surface, multiple random locations were analyzed across the surface of the film, in order to identify the minimum and maximum values of the range of PL energies of the GaN QWs, which should correlate with the maximum and minimum values of the strain, respectively. This spatial sampling resulted in a set of PL spectra between \sim 2.90 eV and \sim 3.04 eV. As seen in Fig. 4a, these spectra were sorted and qualitatively assigned to areas of different crack densities. Higher crack density results in low residual tensile (compressive) in-plane (out-of-plane) strain in the AlN layers and high compressive (tensile) in-plane (out-of-plane) strain in the GaN layers, creating an environment of nonuniform pressure within the GaN OW layers of the superlattice. The quantum confined Stark effect sensitively affects the optical properties of the GaN MQWs, therefore the consequent variation of the piezoelectric polarization within the polar GaN QWs shifts the Γ and HH energy levels. These effects have been shown to result in a linear shift of the PL with strain for similar samples

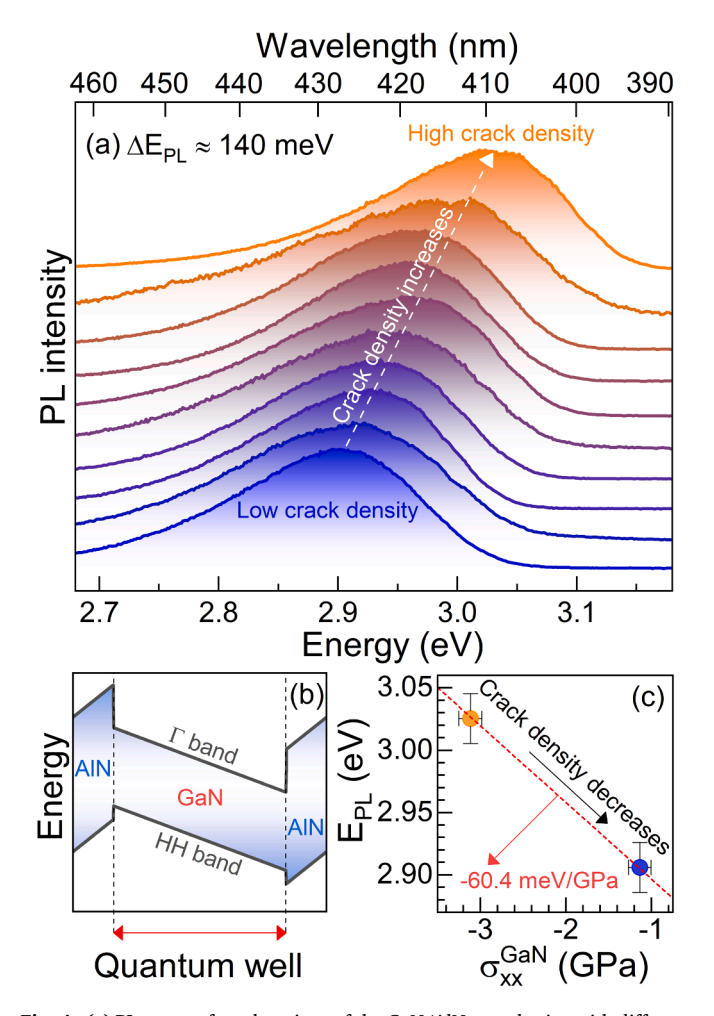


Fig. 4. (a) PL spectra from locations of the GaN/AlN superlattice with different crack density. (b) Schematic diagram of the band structure along one period of the superlattice. (c) Evolution of the photoluminescence emission due to different levels of in-plane stress in the superlattice.

by Kaminska et al. [42]. For our samples, this has resulted in the ~ 140 meV shift in PL seen in Fig. 4a. Areas of high (low) strain in the GaN QWs result from low (high) crack densities, exhibiting a large (small) shift in GaN PL emission. The schematic diagram of the band structure along one period of the superlattice is presented in Fig. 4b. As shown in Figs. 2 and 3, the observed range of in-plane compressive strain in the GaN layers of the superlattice is approximately -0.4×10^{-2} between areas of low and high crack density. This value is equivalent to a variation of about 2.4 GPa in the stressed condition of the in-plane lattice constant of the GaN layers. Based on the linear approximation of the susceptibility of physical parameters of GaN/AlN systems to pressure defined by Strak et al. using ab initio calculations [40], the variation in PL emission was associated to the change in stress by $\Delta E_{\Gamma - HH}/\Delta p \simeq -60.4$ meV/GPa for the 7 nm thick GaN layers of the GaN/AlN superlattice. The distribution of values of PL emission and stress is shown in Fig. 4c, where the error bars originate from the experimental measurements.

This estimated value of -60.4 meV/GPa is very similar to the predicted value of -61.5 meV/GPa from Kaminska et al. [22] that was calculated from density functional theory using the Vienna ab Initio Simulation Package considering hydrostatic strain and the effects of screening of the built-in electric field by free carriers in a 40-period GaN/AlN superlattice with 6 nm (4 nm) thick GaN (AlN) layers. In fact, for wider wells, the experimental results of Ref. [22] no longer matched their theoretical predictions, which matched quite well for narrower well. This was proposed to be the result of the luminescence in the wide QWs being governed mainly by defects due to the greatly reduced oscillator strengths and indirect nature of the excitons in the wide wells. This dramatically reduced the observed lifetime and lessened the influence of increased pressure. Samples in Ref. [22] were grown on AlN templates with the GaN QWs of the superlattice doped with Si to greater than $10^{19}~{\rm cm}^{-3}$. Our sample was grown on a GaN template with no doping. These differences should account for more than an order of magnitude less threading dislocations [14] in regions far from the observable cracks and many orders less point defects in our QW layers, respectively. As a result, we believe this expected dramatic reduction in defects allows for our results to more closely represent the ideal theory of the wide QW as set forth by Kaminska et al. [22]. Different values, such as 43.7 meV/GPa [43], 38.9 meV/GPa [44] and 11.7 meV/GPa [45] have been reported respectively for GaN in the form of microcrystals, a 3 μm thick bulk-like film, and 4 nm thick QWs in a 3 period superlattice of GaN/AlGaN.

4. Conclusion

In this study, we explored cracked, 7 nm thick, polar GaN/AlN multiquantum wells (MQWs) grown on a GaN(0001)/sapphire template to analyze how pressure affects the photoluminescence (PL) energy. As observed through micro-Raman spectroscopy and X-ray diffraction mapping, the strained structure, which had relaxed via crack formation, demonstrated an uneven stress distribution along the film, indicating a correlation between crack spacing and strain. Based on this, we developed a 2D model for calculating the in-plane strain variation in the GaN and AlN layers. The measured values of compressive in-plane strain in the GaN QWs measured away from the cracks varied from -0.4 % in an area of low crack density, to -0.7 % in an area of high crack density. PL from the GaN QWs exhibited energy shift of \sim 140 meV, which was correlated with the difference in strain values across the surface of the sample. As a result, we experimentally determined a pressure coefficient of the PL energy of -60.4 meV/GPa for the 7 nm thick polar GaN QWs. This agrees well with the previously predicted theoretical results, which were demonstrated to break down for such wide QWs. This is generally understood to be the result of growing a more idealized structure, reducing both point defects and extended defects by not doping the QWs and growth on a GaN template, respectively. Therefore, our work indicates that cracks can be utilized for investigating fundamental material properties related to strain effects in nanostructures.

CRediT authorship contribution statement

Fernando M. de Oliveira: Conceptualization, Data curation, Formal analysis, Writing – original draft, Writing – review & editing. Andrian V. Kuchuk: Writing – original draft, Formal analysis, Data curation, Conceptualization, Writing – review & editing. Pijush K. Ghosh: Resources. Morgan E. Ware: Conceptualization, Formal analysis, Writing – original draft, Writing – review & editing. Yuriy I. Mazur: Conceptualization, Formal analysis, Writing – original draft, Writing – review & editing. Gregory J. Salamo: Funding acquisition, Project administration, Supervision.

Declaration of competing interest

The authors declare that they have no known competing financial interests or personal relationships that could have appeared to influence the work reported in this paper.

Data availability

Data will be made available on request.

Supplementary materials

Supplementary material associated with this article can be found, in the online version, at doi:10.1016/j.surfin.2024.104358.

References

- F. Chen, X. Ji, S.P. Lau, Recent progress in group III-nitride nanostructures: From materials to applications, Mater. Sci. Eng.: R: Rep. 142 (2020) 100578, https://doi. org/10.1016/j.mser.2020.100578.
- [2] J. Hao, L. Li, P. Gao, X. Jiang, C. Ban, N. Shi, Deep ultraviolet detectors based on wide bandgap semiconductors: a review, J. Nanopart. Res. 25 (2023) 81, https:// doi.org/10.1007/s11051-023-05694-6.
- [3] Q. Hua, X. Cui, K. Ji, B. Wang, W. Hu, Piezotronics enabled artificial intelligence systems, J. Phys.: Mater. 4 (2021) 022003, https://doi.org/10.1088/2515-7639/ abe55f
- [4] Z. Mu, A. Rasmita, J. Yang, X. Li, W. Gao, Room-Temperature Solid-State Quantum Emitters in the Telecom Range, Adv. Quantum. Technol. 4 (2021) 2100076, https://doi.org/10.1002/qute.202100076.
- [5] S. Lin, D. Wang, Y. Tong, B. Shen, X. Wang, III-nitrides based resonant tunneling diodes, J. Phys. D: Appl. Phys. 53 (2020) 253002, https://doi.org/10.1088/1361-6463/d.PPT1
- [6] R. Islam, S.S.H. Rafin, O.A. Mohammed, Comprehensive Review of Power Electronic Converters in Electric Vehicle Applications, Forecasting 5 (2022) 22–80, https://doi.org/10.3390/forecast5010002.
- [7] S. Liang, G. Wang, T. Tao, F. Xu, K. Chen, T. Zhi, Z. Zhu, W. Chen, Y. Li, K. Xu, B. Liu, GaN-based cascade Micro light-emitting diode in parallel and series arrays for visible light communication, IEEE Photonics. J. 15 (2023) 8200604, https://doi.org/10.1109/JPHOT.2023.3278671.
- [8] S. Tripathy, S.J. Chua, P. Chen, Z.L. Miao, Micro-Raman investigation of strain in GaN and Al x Ga 1 – x N/GaN heterostructures grown on Si (111), J. Appl. Phys. 92 (2002) 3503–3510, https://doi.org/10.1063/1.1502921.
- [9] K. Wang, R.R. Reeber, Thermal residual stress modeling in AlN and GaN multi layer samples, MRS Internet J. Nitride Semicond. Res. 4 (1999) 209–214, https://doi. org/10.1557/S1092578300002477.
- [10] S.J. Hearne, J. Han, S.R. Lee, J.A. Floro, D.M. Follstaedt, E. Chason, I.S.T. Tsong, Brittle-ductile relaxation kinetics of strained AlGaN/GaN heterostructures, Appl. Phys. Lett. 76 (2000) 1534–1536, https://doi.org/10.1063/1.126087.
- [11] J.A. Floro, D.M. Follstaedt, P. Provencio, S.J. Hearne, S.R. Lee, Misfit dislocation formation in the AlGaN/ GaN heterointerface, J. Appl. Phys. 96 (2004) 7087–7094, https://doi.org/10.1063/1.1812361.
- [12] M. Aqib, S. Pouladi, M. Moradnia, R.P.R. Kumar, N. Kim, J. Ryou, Strain accumulation and relaxation on crack formation in epitaxial AlN film on Si (111) substrate, Appl. Phys. Lett. 124 (2024) 042109, https://doi.org/10.1063/ 5.0191258
- [13] X.Q. Shen, T. Takahashi, T. Ide, M. Shimizu, Mechanisms of the micro-crack generation in an ultra-thin AlN/GaN superlattice structure grown on Si (110) substrates by metalorganic chemical vapor deposition, J. Appl. Phys. 118 (2015) 125307. https://doi.org/10.1063/1.4931671.
- [14] V.P. Kladko, A.V. Kuchuk, N.V. Safryuk, V.F. Machulin, P.M. Lytvyn, V. G. Raicheva, A.E. Belyaev, Y.I. Mazur, E.A. DeCuir Jr, M.E. Ware, M.O. Manasreh, Influence of template type and buffer strain on structural properties of GaN multilayer quantum wells grown by PAMBE, an x-ray study, J. Phys. D: Appl. Phys. 44 (2010) 025403, https://doi.org/10.1088/0022-3727/44/2/025403.

- [15] Y. Kotsar, B. Doisneau, E. Bellet-Amalric, A. Das, E. Sarigiannidou, E. Monroy, Strain relaxation in GaN/AlxGa1-xN superlattices grown by plasma-assisted molecular-beam epitaxy, J. Appl. Phys. 110 (2011) 033501, https://doi.org/ 10.1063/1.3618680
- [16] H.V. Stanchu, A.V. Kuchuk, P.M. Lytvyn, Y.I. Mazur, Y. Maidaniuk, M. Benamara, S. Li, S. Kryvyi, V.P. Kladko, A.E. Belyaev, Z.M. Wang, Strain relaxation in GaN/AlN superlattices on GaN (0001) substrate: Combined superlattice-to-substrate lattice misfit and thickness-dependent effects, Mater. Des. 157 (2018) 141–150, https://doi.org/10.1016/j.matdes.2018.07.037.
- [17] F. Bernardini, V. Fiorentini, D. Vanderbilt, Spontaneous polarization and piezoelectric constants of III-V nitrides, Phys. Rev. B 56 (1997) R10024, https://doi.org/10.1103/PhysRevB.56.R10024.
- [18] G. Martin, A. Botchkarev, A. Rockett, H. Morkoc, Valence-band discontinuities of wurtzite GaN, AlN, and InN heterojunctions measured by x-ray photoemission spectroscopy, Appl. Phys. Lett. 68 (1996) 2541–2543, https://doi.org/10.1063/ 1.116177
- [19] V. Kladko, A. Kuchuk, A. Naumov, N. Safriuk, O. Kolomys, S. Kryvyi, H. Stanchu, A. Belyaev, V. Strelchuk, B. Yavich, Y.I. Mazur, M.E. Ware, G.J. Salamo, Effect of strain-polarization fields on optical transitions in AlGaN/GaN multi-quantum well structures, Physica E 76 (2016) 140–145, https://doi.org/10.1016/j.
- [20] S. Schlichting, G.M.O. Hönig, J. Müßener, P. Hille, T. Grieb, S. Westerkamp, J. Teubert, J. Schörmann, M.R. Wagner, A. Rosenauer, M. Eickhoff, Suppression of the quantum-confined Stark effect in polar nitride heterostructures, Commun. Phys. 1 (2018) 48, https://doi.org/10.1038/s42005-018-0044-1.
- [21] C. Zhang, Y. Wu, B. Xia, P. Su, J. Ma, Improvement in quantum efficiency of green GaN-based micro-LED by trapezoidal quantum well, J. Lumin. 263 (2023) 120027, https://doi.org/10.1016/j.jlumin.2023.120027.
- [22] A. Kaminska, D. Jankowski, P. Strak, K.P. Korona, M. Beeler, K. Sakowski, E. Grzanka, J. Borysiuk, K. Sobczak, E. Monroy, S. Krukowski, High pressure and time resolved studies of optical properties of n-type doped GaN/AlN multiquantum wells: Experimental and theoretical analysis, J. Appl. Phys. 120 (2016) 095705, https://doi.org/10.1063/1.4962282.
- [23] Y. Oussaifi, A. Said, A.B. Fredj, L. Debbichi, D. Ceresoli, M. Said, Effect of pressure on the energy band gaps of wurtzite GaN and AlN and electronic properties of their ternary alloys Al_xGa_{1-x}N, Physica B 407 (2012) 3604–3609, https://doi.org/ 10.1016/j.physb.2012.05.035.
- [24] W. Shan, T.J. Schmidt, R.J. Hauenstein, J.J. Song, B. Goldenberg, Pressure-dependent photoluminescence study of wurtzite GaN, Appl. Phys. Lett. 66 (1995) 3492–3494. https://doi.org/10.1063/1.113774.
- [25] A.V. Kuchuk, F.M. de Oliveira, P.K. Ghosh, Y.I. Mazur, H.V. Stanchu, M. D. Teodoro, M.E. Ware, G.J. Salamo, Coherent-interface-induced strain in large lattice-mismatched materials: A new approach for modeling Raman shift, Nano Res. 15 (2022) 2405–2412, https://doi.org/10.1007/s12274-021-3855-4.
- [26] K. Adachi, H. Ogi, A. Nagakubo, N. Nakamura, M. Hirao, M. Imade, M. Yoshimura, Y. Mori, Elastic constants of GaN between 10 and 305K, J. Appl. Phys. 119 (2016) 245111. https://doi.org/10.1063/1.4955046.
- [27] A.F. Wright, Elastic properties of zinc-blende and wurtzite AlN, GaN, and InN, J. Appl. Phys. 82 (1997) 2833, https://doi.org/10.1063/1.366114.
- [28] S. Kryvyi, H. Stanchu, O. Liubchenko, N. Safriuk-Romanenko, A. Kuchuk, A. Wierzbicka, M. Sobanska, A. Reszka, Z.R. Zytkiewicz, V. Kladko, Alternative Route of Fracturing in GaN Films Formed by Nanowires Coalescence on Si Substrate, Cryst. Growth Des. 22 (2022) 3264–3270, https://doi.org/10.1021/acs. crd/2c00104
- [29] L. Huang, H. Sun, L. Sun, K. Shi, Y. Chen, X. Ren, Y. Ge, D. Jiang, X. Liu, W. Knoll, Q. Zhang, Rapid, label-free histopathological diagnosis of liver cancer based on Raman spectroscopy and deep learning, Nat. Commun. 14 (2023) 48, https://doi.org/10.1038/s41467-022-35696-2.

- [30] L. Nasdala, C. Schmidt, Applications of Raman spectroscopy in mineralogy and geochemistry, Elements 16 (2020) 99–104, https://doi.org/10.2138/ geolements 16 2 00
- [31] A. Corpolongo, R.S. Jakubek, A.S. Burton, A.J. Brown, A. Yanchilina, A.D. Czaja, A. Steele, B.V. Wogsland, C. Lee, D. Flannery, D. Baker. E. A. Cloutis, E. Cardarelli, E.L. Scheller, E.L. Berger, F.M. McCubbin, J.R. Hollis, K. Hickman-Lewis, K. Steadman, K. Uckert, L. DeFlores, L. Kah, L.W. Beegle, M. Fries, M. Minitti, N. C. Haney, P. Conrad, R.V. Morris, R. Bhartia, R. Roppel, S. Siljeström, S.A. Asher, S. V. Bykov, S. Sharma, S. Shkolyar, T. Fornaro, W. Abbey, SHERLOC Raman mineral class detections of the Mars 2020 Crater Floor Campaign, J. Geophys. Res.: Planets 128 (2023) e2022JE007455, https://doi.org/10.1029/2022JE007455.
- [32] S.R. Swanson, On the mechanics of microcracking in fiber composite laminates under combined stress, J. Eng. Mater. Technol. 111 (1989) 145–149, https://doi. org/10.1115/1.3226446.
- [33] J.H. Selverian, D. O'Neil, Strength and toughness measurement of thin brittle coatings on substrates Part I. Theory and measurement, Thin. Solid. Films. 235 (1993) 120–128, https://doi.org/10.1016/0040-6090(93)90254-M.
- [34] C. Galiotis, A. Paipetis, Definition and measurement of the shear-lag parameter, β , as an index of the stress transfer efficiency in polymer composites, J. Mater. Sci. 33 (1998) 1137–1143, https://doi.org/10.1023/A:1004357121802.
- [35] M.A. Moram, Z.H. Barber, C.J. Humphreys, Accurate experimental determination of the Poisson's ratio of GaN using high-resolution x-ray diffraction, J. Appl. Phys. 102 (2007) 023505, https://doi.org/10.1063/1.2749484.
- [36] J.M. Wagner, F. Bechstedt, Properties of strained wurtzite GaN and AlN: Ab initio studies, Phys. Rev. B 66 (2002) 115202, https://doi.org/10.1103/ PhysRevB 66 115202
- [37] S.B. Kryvyi, P.M. Lytvyn, V.P. Kladko, H.V. Stanchu, A.V. Kuchuk, Y.I. Mazur, G. J. Salamo, S. Li, P.P. Kogutyuk, A.E. Belyaev, Effect of well/barrier thickness ratio on strain relaxation in GaN/AlN superlattices grown on GaN/sapphire template, J. Vac. Sci. Technol. B 35 (2017) 062902, https://doi.org/10.1116/1.4999468.
- [38] M.A. Moram, M.E. Vickers, X-ray diffraction of III-nitrides, Rep. Prog. Phys. 72 (2009) 036502, https://doi.org/10.1088/0034-4885/72/3/036502.
- [39] M.K. Mahata, S. Ghosh, S.K. Jana, A. Chakraborty, A. Bag, P. Mukhopadhyay, R. Kumar, D. Biswas, Comprehensive strain and band gap analysis of PA-MBE grown AlGaN/GaN heterostructures on sapphire with ultra thin buffer, AIP. Adv. 4 (2014) 117120, https://doi.org/10.1063/1.4902090.
- [40] P. Strak, K. Sakowski, A. Kaminska, S. Krukowski, Influence of pressure on the properties of GaN/AlN multi-quantum wells—Ab initio study, J. Phys. Chem. Solids 93 (2016) 100–117, https://doi.org/10.1016/j.jpcs.2016.02.014.
- [41] S.H. Wei, A. Zunger, Predicted band-gap pressure coefficients of all diamond and zinc-blende semiconductors: Chemical trends, Phys. Rev. B 60 (1999) 5404, https://doi.org/10.1103/PhysRevB.60.5404.
- [42] A. Kaminska, K. Koronski, P. Strak, K. Sobczak, E. Monroy, S. Krukowski, Wurtzite quantum well structures under high pressure, J. Appl. Phys. 128 (2020) 050901, https://doi.org/10.1063/5.0004919.
- [43] M. Steube, K. Reimann, O. Brandt, H. Yang, K.H. Plogg, High pressure luminescence of zincblende and wurtzite GaN, Phys. Status Solidi B 211 (1999) 57–61, https://doi.org/10.1002/(SICI)1521-3951(199901)211:1<57::AID-PSSB57-3.0.CO:2-V.</p>
- [44] P. Perlin, L. Mattos, N.A. Shapiro, J. Kruger, W.S. Wong, T. Sands, N.W. Cheung, E. R. Weber, Reduction of the energy gap pressure coefficient of GaN due to the constraining presence of the sapphire substrate, J. Appl. Phys. 85 (1999) 2385–2389, https://doi.org/10.1063/1.369554.
- [45] H. Teisseyre, A. Kamińska, G. Franssen, A. Dussaigne, N. Grandjean, I. Grzegory, B. Łucznik, T. Suski, Different pressure behavior of GaN/AlGaN quantum structures grown along polar and nonpolar crystallographic directions, J. Appl. Phys. 105 (2009) 063104, https://doi.org/10.1063/1.3043888.